Separation Science and Technology
Publication details, including instructions for authors and subscription information:
http://www.informaworld.com/smpp/title~content=t713708471

ION EXCHANGE OF SEVERAL RADIONUCLIDES ON THE HYDROUS CRYSTALLINE SILICOTITANATE, UOP IONSIV IE-911

M. E. Huckman[a]; I. M. Latheef[a]; R. G. Anthony[a]
[a] Department of Chemical Engineering, Kinetics, Catalysis, and Reaction Engineering Laboratory, Texas A&M University, College Station, TX

To cite this Article Huckman, M. E. , Latheef, I. M. and Anthony, R. G.(1999) 'ION EXCHANGE OF SEVERAL RADIONUCLIDES ON THE HYDROUS CRYSTALLINE SILICOTITANATE, UOP IONSIV IE-911', Separation Science and Technology, 34: 6, 1145 — 1166
To link to this Article: DOI: 10.1080/01496399908951086
URL: http://dx.doi.org/10.1080/01496399908951086

SEPARATION SCIENCE AND TECHNOLOGY, 34(6&7), pp. 1145–1166, 1999

ION EXCHANGE OF SEVERAL RADIONUCLIDES ON THE HYDROUS CRYSTALLINE SILICOTITANATE, UOP IONSIV IE-911

M. E. Huckman, I. M. Latheef, R. G. Anthony
Kinetics, Catalysis, and Reaction Engineering Laboratory
Department of Chemical Engineering
Texas A&M University, College Station, TX 77843

ABSTRACT

The crystalline silicotitanate, UOP IONSIV IE-911, is a proven material for removing radionuclides from a wide variety of waste streams. It is superior for removing several radionuclides from the highly alkaline solutions typical of DOE wastes. Our laboratory previously developed an equilibrium model applicable to complex solutions for IE-910 (the powder form of the granular IE-911), and more recently, we have developed several single component ion-exchange kinetic models for predicting column breakthrough curves and batch reactor concentration histories. In this paper, we model ion-exchange column performance using effective diffusivities determined from batch kinetic experiments. This technique is preferable because the batch

experiments are easier, faster, and cheaper to perform than column experiments. We also extend these ideas to multicomponent systems. Finally, we evaluate the ability of our equilibrium model to predict data for IE-911.

INTRODUCTION

Department of Energy (DOE) radioactive waste streams can contain several radionuclides, including cesium, rubidium, and strontium. Cesium is of particular importance because it is a gamma emitter and has a long half-life. These radionuclides also have high mobilities in the biosphere (1). Ion exchange is a viable technology for removing radionuclides from such waste streams. The resulting radioactive solid can be vitrified into glass logs and ultimately stored in high-level waste federal geologic repositories (2-4), while the liquid can be disposed of as low-level waste. A number of ion-exchange materials have been evaluated for this application, and the crystalline silicotitanate (CST), UOP IONSIV IE-911, has emerged as a superior candidate (5-7). This recently synthesized CST (8) not only has a high selectivity for Cs^+ and several other radionuclides in highly alkaline solutions but also is stable under high levels of radiation (9). To design an efficient treatment technology using IE-911, an understanding of the ion exchange kinetics is essential. From this understanding, it is possible to develop a mathematical model of the process which can then be used to design an industrial application.

The major components of an ion-exchange model include: a) a differential material balance around the particle, b) a constitutive equation for diffusive flux, c) a differential material balance for the bulk liquid, and d) equilibrium data relating the concentration in the exchange material to the concentration in the liquid phase (10).

In this study, a two-phase homogeneous balance using only one diffusion coefficient is written around the particle and Fick's law is used for the flux. This form of the particle material balance has been shown to yield good results for these types of systems (11). The bulk liquid material balance varies, depending on whether a batch

or a column reactor is being used. The column balance includes terms to account for dispersion and film resistance to mass transfer. A Langmuir isotherm is used to fit the experimental equilibrium data. The experimental data are also compared with the predictions from an equilibrium model previously developed in our laboratory (12). This model was developed based on data for IE-910, the powder form of IE-911.

In theory, the effective diffusivity can be determined from either batch kinetic data or column breakthrough curves. In practice, the batch experiments are easier, quicker, and cheaper to perform than column experiments. Moreover, dispersion and film resistance, which can be important in column experiments, affect the breakthrough curve and make it difficult to accurately determine the effective diffusivity. Thus, it is preferable to measure the effective diffusivity using batch experiments, and then use this value to predict column behavior.

EQUILIBRIUM ISOTHERM

Equilibrium data for Cs^+ and Rb^+ were obtained for a solution containing 0.6 *M* NaOH plus 0.4 *M* $NaNO_3$ (for a total sodium concentration of 1 *M*). A known mass of IE-911 was added to a known volume of solution containing a known initial concentration of one of the radionuclides. (Nonradioactive isotopes were used for all experiments.) The mixture was shaken for 72 h and the final liquid concentration was measured by flame atomic absorption using a Varian Atomic Absorption

Spectrophotometer, model SpectrAA-30. The concentration in the solid was calculated from the initial and final liquid concentrations. Either the initial concentration or the solid/liquid ratio was varied to generate a variety of equilibrium data points. Also, the previously developed equilibrium model was used to predict the equilibrium for this solution in the same concentration range (12).

Figures 1 and 2 show the experimental results, along with the equilibrium model predictions for Cs^+ and Rb^+. These figures indicate that the equilibrium model is in

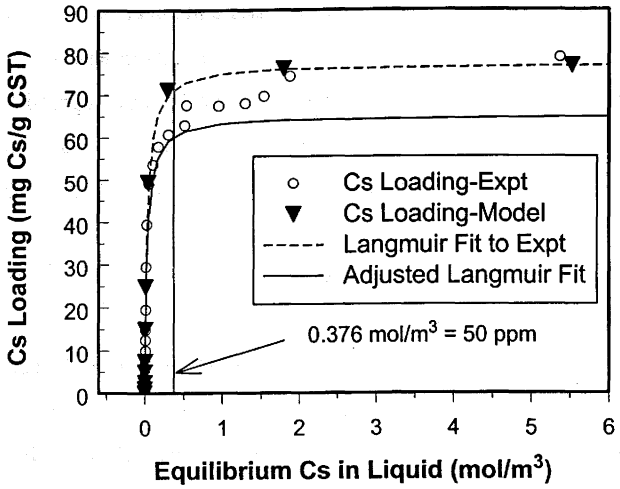

FIGURE 1. Plot of Cs^+ equilibrium isotherm for IONSIV IE911 in 1 *M* Na^+ solution. Shown are the experimental data, the model-generated data, a Langmuir isotherm fit to experiment, and the adjusted isotherm used in the kinetic model. The vertical line indicates the feed concentration for the column experiments.

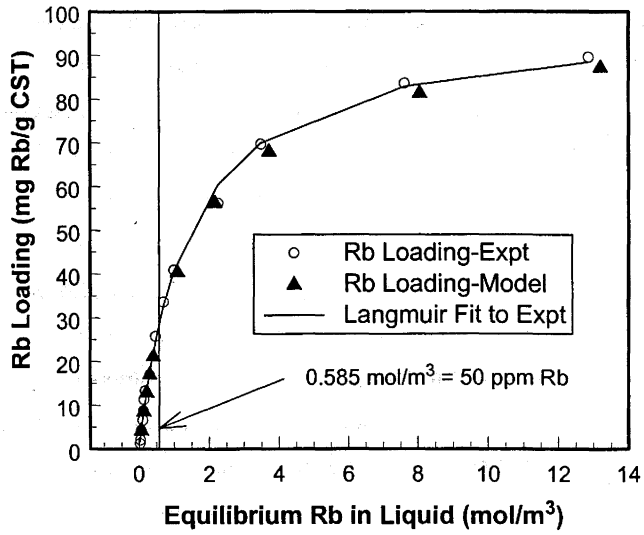

FIGURE 2. Plot of Rb^+ equilibrium isotherm for IONSIV IE911 in 1 *M* Na^+ solution. Shown are the experimental data, the model-generated data, and the Langmuir isotherm fit to the experiments. This isotherm was used in the kinetic models.

good agreement with the experimental data over a large range of liquid concentrations. The figures also show Langmuir isotherm(s) fit to the experimental data. The Langmuir isotherm applies to adsorption in ideal solutions but does not necessarily hold for ion-exchange systems. However, it has the appropriate shape and is convenient for use in kinetic models so it is used as a fitting function. The Langmuir parameters were determined by minimizing the squared difference between experiment and isotherm over the entire liquid concentration range.

The Cs^+ equilibrium data have a sharp "elbow" in the neighborhood of 50 ppm - the operating range for the kinetic experiments - and the Langmuir isotherm does not fit the data well in this region. To achieve accurate predictions in the operating region, the Langmuir parameter, q_{Cs}^T, was decreased and this *adjusted* isotherm was used in the kinetic models. The Rb^+ data do not exhibit this sharp elbow, and the Langmuir isotherm fits well in the operating region. Hence, the Rb^+ isotherm was not adjusted. The adjusted isotherms do not fit the data as well as the original isotherm over the entire region; however, they do provide a better fit in the region where the kinetic experiments were performed.

Experimental data were not available for Sr^{2+}, so that isotherm was determined using only model-generated data. The shape of the Sr^{2+} isotherm is similar to that of Cs^+.

An equilibrium value, extracted from a Sr^{2+} column experiment, indicated that the isotherm overpredicted the solid capacity for a liquid concentration of 50 ppm. Since this is similar to the discrepancies found for Cs^+ in the 50-ppm range, the Langmuir parameter, q_{Sr}^T, was decreased so that the isotherm matched the value from the column experiment. The model data and both isotherms are shown in Figure 3. The isotherm parameters for all cases are summarized in Table 1.

To develop accurate kinetic models over a larger concentration range, an improved isotherm is desirable. For these types of experiments, the authors suggest using a

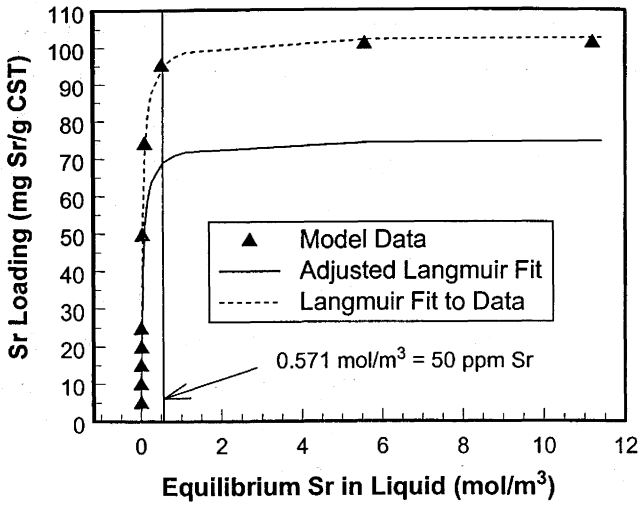

FIGURE 3. Plot of Sr^{2+} equilibrium isotherm for IONSIV IE911 in 1 *M* Na^{+} solution. Shown are the model-generated data, a Langmuir isotherm fit to these data, and the adjusted isotherm used in the kinetic model. The vertical line indicates the feed concentration for the column experiments.

TABLE 1. SUMMARY OF PARAMETERS USED IN THE LANGMUIR ISOTHERMS.

(both the q^t determined from the data and the adjusted values used in the kinetic models.)

Cation	K_{ii} (m^3/mol)	Original q_i^T (mg/g)	Adjusted q_i^T (mg/g)	n
Cs^+	32.4	77.1	65	-
Cs^+ (mod.)	42.6	71.0	-	0.95
Rb^+	0.71	98.2	-	-
Sr^{++}	20.4	103	75	-

modified Langmuir isotherm of the form

$$q_i = \frac{q_i^T K_{ii} C_i}{1 + K_{ii} C_i^n} \quad . \tag{1}$$

When the exponent, n, is 1.0, the traditional Langmuir isotherm is retrieved. Figure 4 shows a modified isotherm fit to the Cs^+ experimental data. This figure illustrates how the exponent allows a better fit in the "elbow" region of the data. The parameters used are shown in Table 1. It should be noted that the experimental data from the kinetic experiments do not cover such a large range of concentrations, and the *adjusted* isotherm was used in the kinetic models.

BATCH EXPERIMENTS

Batch kinetic data were gathered for Cs^+, Sr^{2+} and Rb^+. A diagram of the batch reactor is shown in Figure 5. The IE-911 pellets reside in a pellet holder to prevent mechanical degradation that results from contact with the mixer impeller or the stir bar. The mixer and stir bar keep the bulk solution well mixed and provide significant flow through the pellet holder. Film resistance to mass transfer is considered negligible for this reactor (11).

The pellet holder was filled with 10 g of IE-911 pellets sieved to a known size distribution. Then 900 mL of the 0.6 *M* NaOH - 0.4 *M* $NaNO_3$ solution was added and the reactor was mixed for 8 to 12 h. Next, 100 mL of the same solution containing 1000 ppm of one radionuclide was added. Thus, the initial radionuclide concentration for all experiments was 100 ppm. At known intervals, 3-mL samples were withdrawn from the reactor using a filtering syringe. The radionuclide concentration in these samples was measured using flame atomic absorption. The reaction was stopped after approximately 24 h.

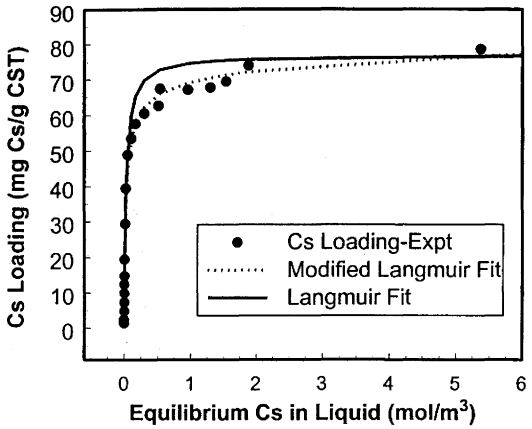

FIGURE 4. Plot of modified Langmuir isotherm for Cs^+ for IONSIV IE911 in 1 *M* Na^+ solution. Shown are the experimental data, the original Langmuir isotherm fit to experiment, and the modified isotherm suggested for use in kinetic model covering a larger range of liquid concentrations.

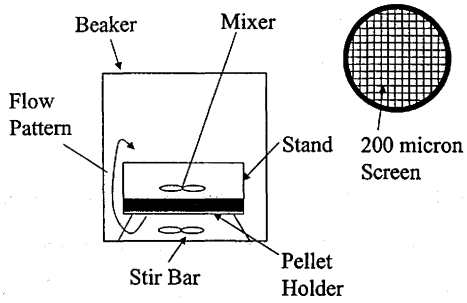

FIGURE 5. Diagram of the reactor used for batch kinetic experiments. A top view of the pellet holder is shown at the right. The pellet holder protects the granules from mechanical degradation. It has a 200 μm screen on the top and the bottom to allow liquid flow through the bed of granules. There is a stir bar below and a mixer impeller above the pellet holder. For the batch experiments, the liquid volume was 1 L and 10 g of IONSIV IE-911 was in the pellet holder.

The two-phase, homogeneous particle material balance used in the batch model is written as

$$\frac{\partial \overline{C_i}}{\partial t}\left[\varepsilon_p + (1-\varepsilon_p)\frac{\partial q_i}{\partial \overline{C_i}}\right] = \frac{1}{r^2}\frac{\partial}{\partial r}\left[r^2 D_e \frac{\partial \overline{C_i}}{\partial r}\right], \tag{2}$$

and the bulk material balance for the batch reactor as

$$\frac{\partial C_i}{\partial t} = \frac{-3M}{R_p \rho_p V_{Rx}} D_e \left.\frac{\partial \overline{C_i}}{\partial r}\right|_{r=R_p}. \tag{3}$$

The solid and liquid concentrations are related through the Langmuir isotherm

$$q_i = \frac{q_i^T K_{ii} C_i}{1 + K_{ii} C_i}. \tag{4}$$

The boundary and initial conditions are

$$@t=0, \quad C_i = C_i^0, \quad \overline{C_i} = 0 \ \forall \ r, \tag{5}$$

$$@r=0, \quad \frac{\partial \overline{C_i}}{\partial r} = 0, \tag{6}$$

$$@r=R_p, \quad \overline{C_i} = C_i. \tag{7}$$

The equations were solved numerically to yield a concentration-versus-time curve.

The spatial derivatives were discretized using second-order finite-difference approximations, and the resulting set of ordinary differential equations was solved using the Runga-Kutta based integration subroutine IVPRK from the IMSL library of

FORTRAN subroutines purchased through Visual Numerics (Houston, TX). The only adjustable parameter in the model is the effective diffusivity.

Figures 6 through 8 show the experimental results, along with model simulations using the best-fit effective diffusivity, D_e. As indicated in the figures, two experiments using ion-exchange particles with different diameters were performed for each radionuclide. The effective diffusivities used to simulate the experiments were 0.9×10^{-10} m^2/s for Cs^+, 1.0×10^{-10} m^2/s for Rb^+, and 0.8×10^{-10} m^2/s for Sr^{++}. The figures indicate that the model matches the experimental data well. (Table 2 summarizes the effective diffusivities used for these simulations as well as the column experiments discussed below.)

The molecular diffusivities of Cs^+ and Rb^+ can be estimated from their ionic conductances at infinite dilution (13,14). These estimates are 2.05×10^{-10} m^2/s for Cs^+ and 2.07×10^{-10} m^2/s for Rb^+ (15). The effective diffusivity, the particle porosity, and the particle tortuosity are related through the formula

$$D_e = \frac{\varepsilon_p D_m}{\tau} \quad . \tag{8}$$

BET data were measured for IE-911 using a Micromeritics ASAP 2000 porosimetry system, and the particle porosity was estimated as 0.23. Thus, the values above indicate an average particle tortuosity of 5.0, which falls within the range

$$\frac{(2-\varepsilon)^2}{\varepsilon} \geq \tau \geq 2 \tag{9}$$

suggested by Helfferich (14).

SINGLE-COMPONENT COLUMN EXPERIMENTS

Single-component column experiments were performed for Cs^+, Rb^+, and Sr^{2+}. The 1 *M* Na^+ solution described previously was used in each experiment. The column was 6

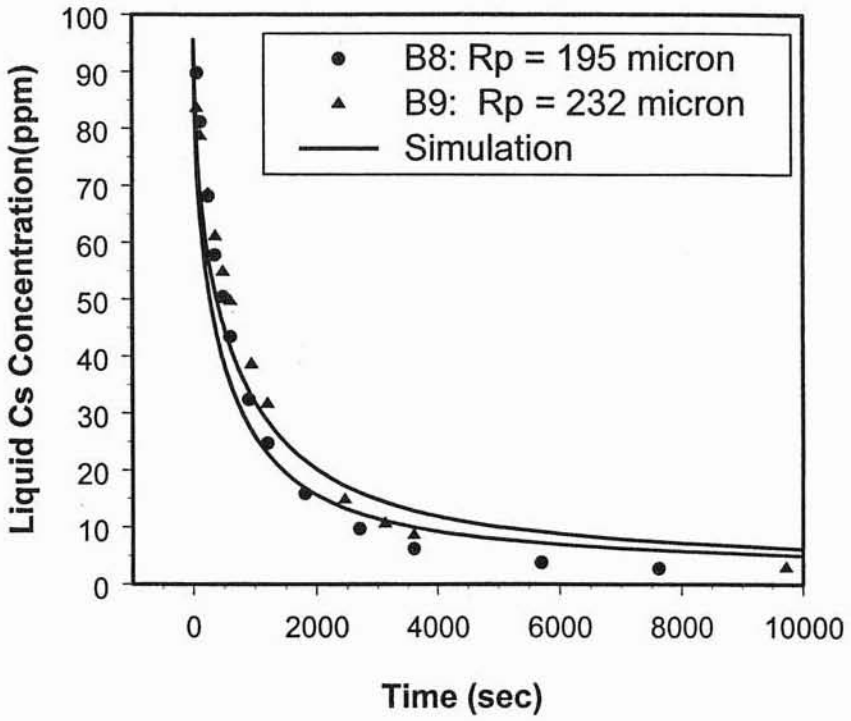

FIGURE 6. Plot of batch kinetic results for Cs^+ on IONSIV IE911 in 1 *M* Na^+ solution Shown are the experimental data for two different pellet sizes along with corresponding model simulations. The initial concentration was 100 mg/L, and the solid/liquid ratio was 100 ml/g.

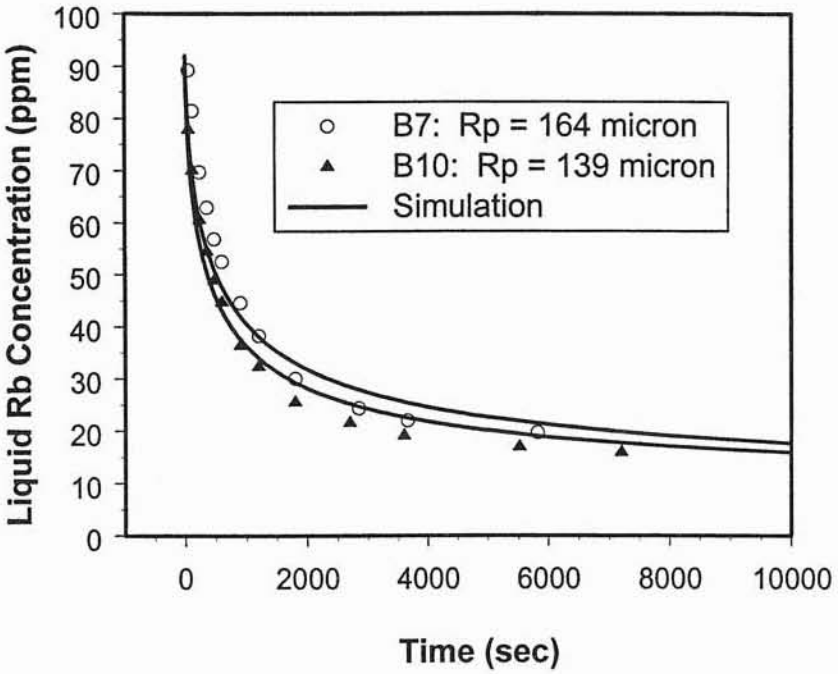

FIGURE 7. Plot of batch kinetic results for Rb^+ on IONSIV IE911 in 1 *M* Na^+ solution. Shown are the experimental data for two different pellet sizes along with corresponding model simulations. The initial concentration was 100 mg/L, and the solid/liquid ratio was 100 mL/g.

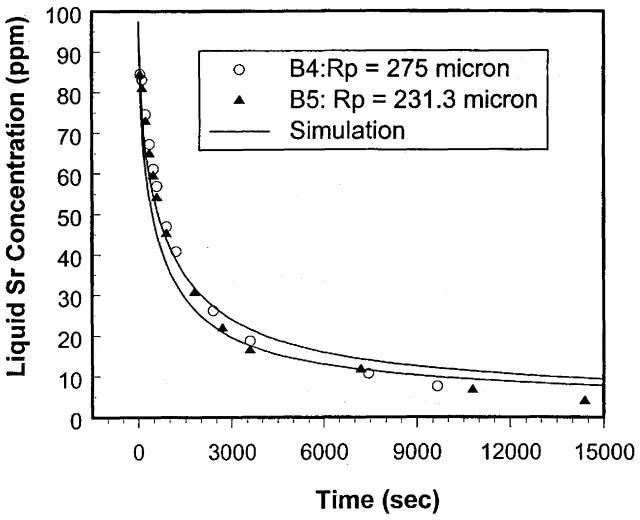

FIGURE 8. Plot of batch kinetic results for Sr^{2+} on IONSIV IE911 in 1 *M* Na^{+} solution. Shown are the experimental data for two different pellet sizes along with corresponding model simulations. The initial concentration was 100 mg/L, and the solid liquid ratio was 100 mL/g.

TABLE 2. SUMMARY OF THE EFFECTIVE DIFFUSIVITIES USED IN THE MODEL SIMULATIONS.

Cation	D_e (m^2/s) batch	D_e (m^2/s) column
Cs^{+}	0.9×10^{-10}	1.0×10^{-10}
Rb^{+}	1.0×10^{-10}	0.9×10^{-10}
Sr^{2+}	0.8×10^{-10}	1.0×10^{-10}

cm long and 1.1 cm in diameter. All experiments were performed at 23°C and are considered isothermal. The average particle radius in each experiments was 188 μm. The loaded bed density was 1.0 g/cm^3. The flowrates were between 3.2 and 3.4 mL/min (33 and 36 column volumes per hour, respectively). Initially, the column was equilibrated with the 1 *M* Na^+ solution without any radionuclide; then a concentration step change was introduced. The initial radionuclide concentration for all experiments was 50 ppm. The column effluent was periodically sampled, and the radionuclide concentration was determined using flame atomic absorption.

The bulk material balance for the column model is written as

$$\frac{\partial C_i}{\partial t} = -v_i \frac{\partial C_i}{\partial x} + D \frac{\partial^2 C_i}{\partial x^2} - \frac{3}{R_p} k_f \left[C_i - \overline{C_i} \,\big|_{r=R_p} \right] . \tag{10}$$

The particle material balance and the isotherm remain the same as those presented above for the batch model. The initial and boundary conditions were

$$@t=0,\ \overline{C_i} = C_i = 0 \quad \forall\ r \ \wedge\ x \neq 0,\ C_i = C_i^{\,o} \ @x=0\ , \tag{11}$$

$$@r=0\ \ \frac{\partial \overline{C_i}}{\partial r} = 0 \ \forall\ x\ , \tag{12}$$

$$@r=R_p\ \ D_e \frac{\partial \overline{C_i}}{\partial r} = k_f (C_i - \overline{C_i}) \quad \forall\ x\ , \tag{13}$$

$$@x=L\ \ \frac{\partial C_i}{\partial x} = 0\ , \tag{14}$$

$$@x=0\ \ D \frac{\partial C_i}{\partial x} = v_i (C_i - C_i^{\,o})\ . \tag{15}$$

The dispersion coefficient, D, was estimated using the correlation developed by Suzuki and Smith (16). The mass transfer coefficient, k_f, was estimated by using a correlation from Perry's Chemical Engineers' Handbook (17). Again, the only adjustable parameter in the model is the effective diffusivity.

The equations were solved numerically. All spatial derivatives were discretized using orthogonal collocation. In the *x* direction, finite elements are introduced and Jacobi polynomials used to approximate the concentration profile in each element. This method allows a large number of collocation points to be used without the numerical oscillation problems typically encountered when high-order polynomials are used. The first derivatives of the concentration profiles were set equal at the boundaries of the elements. In the *r* direction, Legendre polynomials were used to approximate the particle concentration profile. The resulting system of algebraic and differential equations was solved using the integration package DDASSL (18), which is designed to solve systems of this type. Integration is performed using a fifth-order Adams / Moulton algorithm.

Figures 9 through 11 show the experimental breakthrough curves along with the model simulations. The effective diffusivities used for the model simulations were 1.0×10^{-10} m^2/s, 0.9×10^{-10} m^2/s, and 1.0×10^{-10} m^2/s, for Cs^+, Rb^+, and Sr^{2+}, respectively. As indicated in Table 2, these results differ from the values determined from the batch experiments by 20% or less.

MULTICOMPONENT COLUMN EXPERIMENTS

Multicomponent ion-exchange column experiments were performed for the Cs^+/Rb^+ and the Sr^{2+}/Rb^+ systems. The experimental procedure was identical to that described for the single-component experiments, and the concentration step change was 50 ppm for each radionuclide.

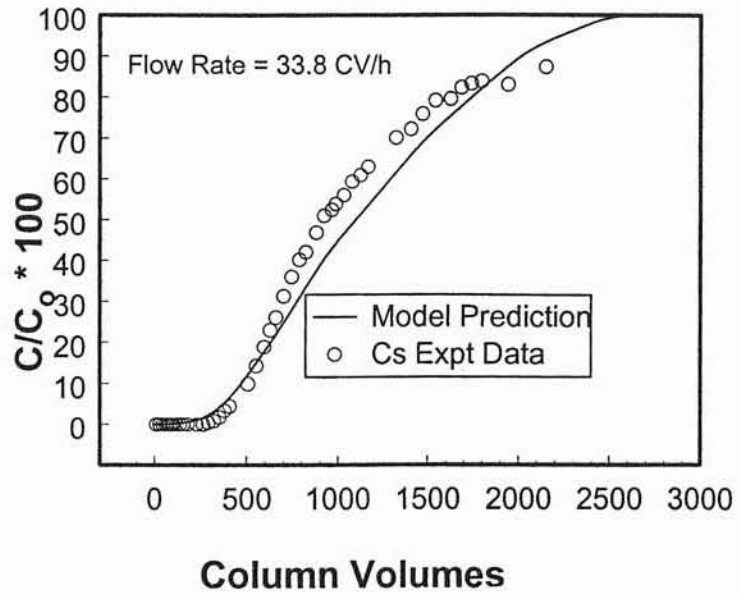

FIGURE 9. Plot of Cs^+ breakthrough curve for IONSIV IE911 in 1 *M* Na^+ solution. Shown are the experimental data along with the model simulation. The feed concentration was 50 mg/L, and the flowrate was 3.2 mL/min.

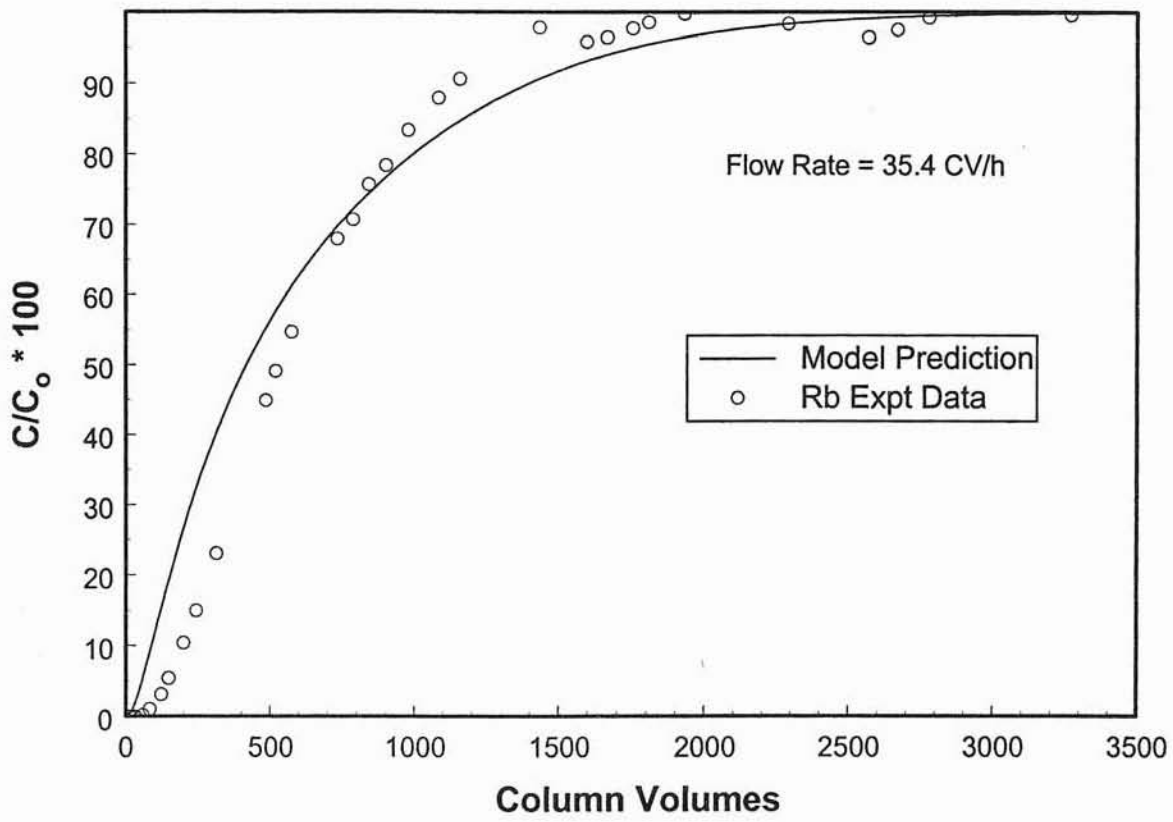

FIGURE 10. Plot of Rb^+ breakthrough curve for IONSIV IE911 in 1 *M* Na^+ solution. Shown are the experimental data along with the model simulation. The feed concentration was 50 mg/L, and the flow rate was 3.4 mL/min.

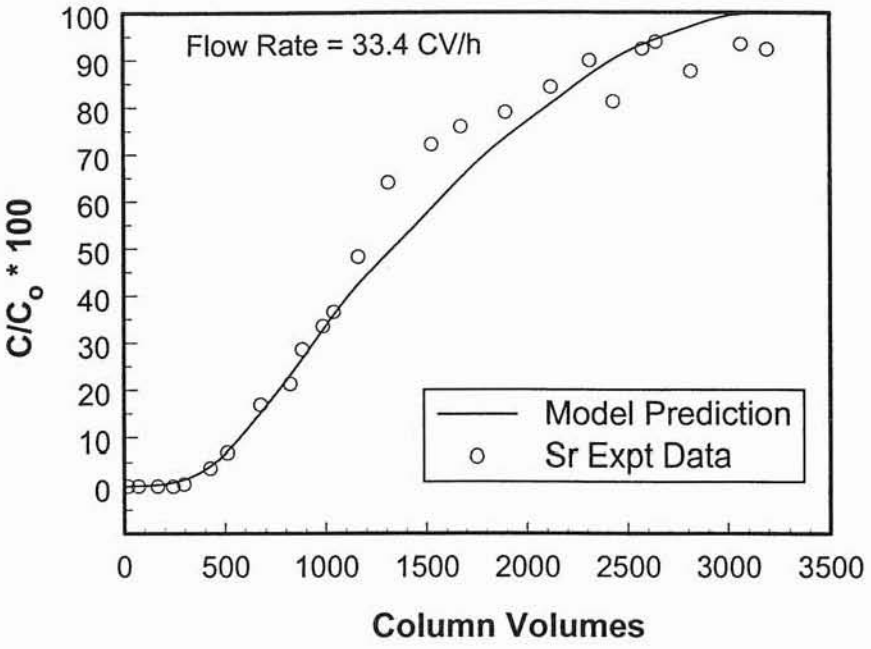

FIGURE 11. Plot of Sr^{2+} breakthrough curve for IONSIV IE911 in 1 *M* Na^+ solution. Shown are the experimental data along the with model simulation. The feed concentration was 50 mg/L, and the flow rate was 3.2 mL/min.

A multicomponent Langmuir isotherm was used to include competitive exchange and is written as

$$q_i = \frac{q_i^T K_{ii} C_i}{1 + K_{ii} C_i + K_{ij} C_j} , \qquad (16)$$

where q_i^T and K_{ii} are the parameters previously determined for the single-component systems. For each multicomponent column experiment, the area to the left of the breakthrough curve can be used to estimate the equilibrium solid concentration, q, for each radionuclide at the feed liquid concentration. The interaction coefficient, K_{ij}, was chosen to match this estimate.

The particle material balance was modified to

$$\frac{\partial \overline{C_i}}{\partial t}\left[\varepsilon_p + (1-\varepsilon_p)\frac{\partial q_i}{\partial \overline{C_i}}\right] + (1-\varepsilon_p)\frac{\partial q_i}{\partial \overline{C_j}}\frac{\partial \overline{C_j}}{\partial t} = \frac{1}{r^2}\frac{\partial}{\partial r}\left[r^2 D_e \frac{\partial \overline{C_i}}{\partial r}\right] . \qquad (17)$$

The new term accounts for movement of component i into, or out of, the solid due to the movement of component j in the liquid. One particle material balance, one bulk material balance, and one isotherm are required for each species.

Thus, for the multicomponent case, the model requires four material balances and two isotherms. These equations were solved numerically using the same techniques described for the single-component column model. Figures 12 and 13 show the experimentally determined breakthrough curves along with the model simulations. The effective diffusivities used for each species are the same as those used for the single-component model simulations. The figures indicate that the simulations match the experimental data well.

The two-phase homogeneous particle balance used in the column model predicts well-behaved particle concentration profiles for single-component experiments. These profiles resemble parabolas, each having the maximum at the particle surface and the minimum at the center. Indeed, these equations are often solved by assuming that the profile is a parabola (19,20). For multicomponent experiments, more complex concentration profiles are possible. Concentration minimums or maximums can occur at points between the particle surface and the center. More collocation points are required to model more complex concentration profiles (21). Figures 12 and 13 indicate that the multicomponent model simulations are not as smooth as the single-component model simulations. In an attempt to improve the simulation results, the number of collocation points in the particle was increased. However, the numerical method became unstable for the multicomponent system when more than three collocation points were used. Presumably, this is caused by the increased order of the trial polynomials.

CONCLUSIONS

Batch and column experiments were performed to examine the kinetics of Cs^+, Rb^+, and Sr^{2+} ion exchange on the CST, UOP IONSIV IE-911. Mathematical models

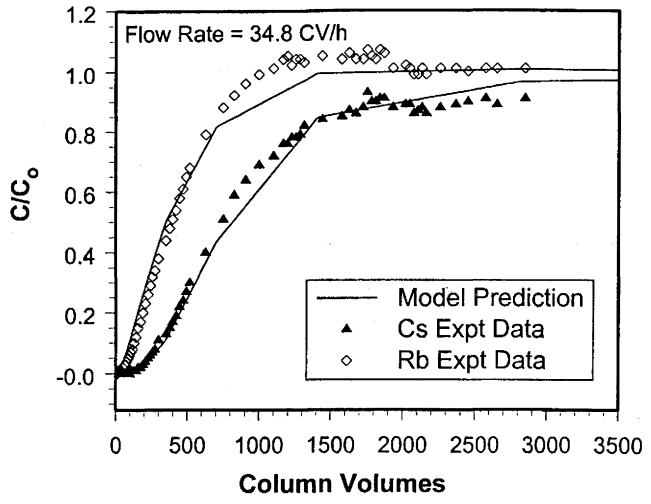

FIGURE 12. Plot of Cs^+/Rb^+ multicomponent breakthrough curves for IONSIV IE911 in 1 M Na^+ solution. Shown are the experimental data along with the model simulation. The feed concentration was 50 mg/L, and the flow rate was 3.3 mL/min.

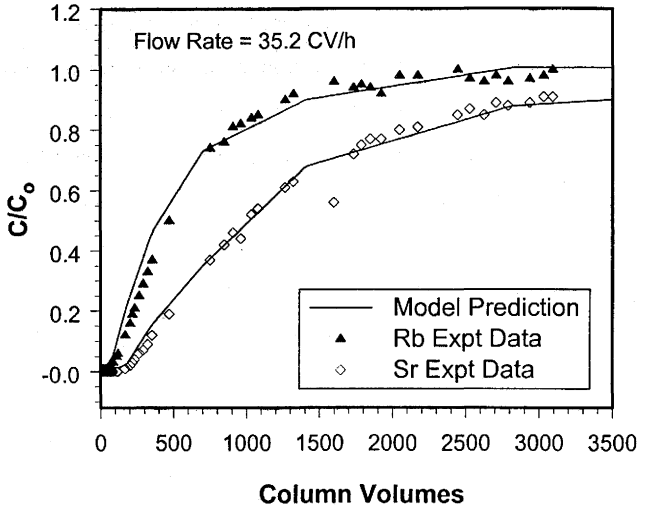

FIGURE 13. Plot of Sr^{2+}/Rb^+ multicomponent breakthrough curves for IONSIV IE911 in 1 *M* Na^+ solution. Shown are the experimental data along with the model simulation. The feed concentration was 50 mg/L, and the flowrate was 3.4 mL/min.

containing one adjustable parameter, the effective diffusivity, were developed to simulate these experiments. This study illustrates that effective diffusivities determined from batch data compare favorably with those determined from column experiments. The batch technique saves time and money as compared with determining the effective diffusivity from column experiments. The values of the effective diffusivities fall within the range expected for diffusion into porous particles.

The study also evaluated the use of effective diffusivities determined from single-component data in a multicomponent column model. The model simulations compared favorably with experimental results. However, the numerical technique required to solve the multicomponent system needs to be more robust.

The equilibrium model previously developed to predict data for IE-910 (the powder form of IE-911) compares favorably with experimental data for IE-911. However, the Langmuir isotherm tends to overpredict the solid concentration when there is a sharp bend in the data. The authors suggest a modified form of the isotherm for use in kinetic models covering a larger range of liquid concentrations.

NOMENCLATURE

C_i bulk liquid concentration of i (mol/m^3)

$\overline{C_i}$ pore liquid concentration of i (mol/m^3)

D dispersion coefficient (m^2/S)

D_e effective diffusivity (m^2/S)

D_m molecular diffusivity (m^2/S)

k_f film mass transfer coefficient (m/S)

K_{ii} single-component Langmuir parameter (m^3/mol)

K_{ij} multicomponent Langmuir parameter (m^3/mol)

L column length (m)

M total mass of particles (kg)

q_i solid-phase concentration of i (mol/m^3)

q_i^T solid capacity of i (mol/m^3)

r spatial variable towards the particle center

R_p average particle radius (m)

v_i interstitial velocity (m/s)

V_{Rx} batch reactor volume (m^3)

x spatial variable along column axis

ε particle porosity

ρ_p particle density (kg/m^3)

τ particle tortuosity

REFERENCES

1. M. Moore, Bull. At. Sci. (March 1993).

2. H. Babad, R. J. Cash, and J. L. Deichman, J. Hazardous Mater. *35*, 427 (1993).

3. R. H. Gray, and C. D. Becker, Environ. Manage. *17*, 461 (1993).

4. D. L. Illman, Chem. Eng. News, p. 3 (June 21, 1993).

5. G. N. Brown, K. J. Carson, J. R. DesChane, and R. J. Elovich, Performance Evaluation of 24 Ion Exchange Materials for Removing Cesium and Strontium from Actual and Simulated N-Reactor Storage Basin Water, Report PNNL-11711, Pacific Northwest National Laboratory, Richland, WA, 1997.

6. G. N. Brown, J. R. Bontha, K. J.Carson, R. J.Elovich, and J. R. DesChane, Comparison of Inorganic Ion Exchange Materials for Removing Cesium, Strontium, and Transuranic Elements from K-Basin Water, Report PNNL-11746, Pacific Northwest National Laboratory, Richland, WA, 1997.

7. G. N. Brown, J. E. Amonette, T. M. Kafka, and S. F. Yates, Efficient Separations and Processing Crosscutting Program: Develop and Test Sorbents, Report PNNL-11451, Pacific Northwest National Laboratory, Richland, WA, 1997.

8. R. G. Anthony, C. V. Philip, and R. G. Dosch, Waste Manage. *13*, 503 (1993).

9. S. F. Marsh, Z. V. Svitra, and S. M. Bowen, Distributions of 14 Elements on 60 Selected Absorbers from Two Simulant Solutions (Acid-Dissolved Sludge and Alkaline Supernate) for Hanford HLW Tank 102-SY, Report LA-12654, Los Alamos National Laboratory, 1993.

10. M. E. Huckman, D. Gu, C. V. Philip, and R. G. Anthony, in *Emerging Separation Technologies for Metal II*, R. G. Bautista, Ed., The Minerals, Metals & Materials Society Press, Warrendale, PA, 1996, p. 135.

11. D. Gu, L. Nguyen, C. V. Philip, M. E. Huckman, R. G. Anthony, Ind. Eng. Chem. Res. *12*(36), 5377 (1997).

12. Z. Zheng, R. G. Anthony, and J. E. Miller, Ind. Eng. Chem. Res. *36*(6), 2427 (1997).

13. E. L. Cussler, *Multicomponent Diffusion*, Elsevier Scientific Publishing Company, New York, 1976.

14. F. Helfferich, in *Ion Exchange*, J .A. Marinsky, ed., Marcel Dekker, Inc., New York, 1966.

15. P. Vanysek, in *Handbook of Chemistry and Physics*, 71st ed., D. R. Lide, Ed., CRC Press, Boston, 1990, p. 5-97.

16. M. Suzuki, and J. M. Smith, Chem. Eng. J. *3*, 256 (1972).

17. T. Vermeulen, M. D. LeVan, and N. K. Hiester, in *Perry's Chemical Engineers' Handbook*, 6th ed., D. W. Green and J. O. Majoney, Eds., McGraw-Hill, New York, 1984, Section 16.

18. L. R. Petzold, A Description of DASSL: A Differential/Algebraic System Solver, Report SAND82-8637, Sandia National Laboratories, 1982.

19. D. D. Do, and R. G. Rice, AIChE J. *32*(1), 149 (1986).

20. P. I. Cen and R. T. Yang, AIChE J. *32*(10), 1635 (1986).

21. B. A. Finlayson, *Nonlinear Analysis in Chemical Engineering*, McGraw-Hill, New York, 1980.